Momentum-Resolved Spin Dynamics of Bulk and Surface Excited States in the Topological Insulator Bi_2Se_3

C. Cacho,[1] A. Crepaldi,[2] M. Battiato,[3] J. Braun,[4] F. Cilento,[2] M. Zacchigna,[5] M. C. Richter,[6,7] O. Heckmann,[6,7] E. Springate,[1] Y. Liu,[8] S. S. Dhesi,[8] H. Berger,[9] Ph. Bugnon,[9] K. Held,[3] M. Grioni,[9] H. Ebert,[4] K. Hricovini,[6,7] J. Minár,[4,10] and F. Parmigiani[2,11,12,*]

[1]*Central Laser Facility, STFC Rutherford Appleton Laboratory, Harwell OX11 0QX, United Kingdom*
[2]*Elettra–Sincrotrone Trieste S. C. p. A., Strada Statale 14, km 163.5, 34149 Basovizza, Trieste, Italy*
[3]*Institute of Solid State Physics, Vienna University of Technology, Wiedner Hauptstrasse 8-10, A 1040 Wien, Austria*
[4]*Department Chemie, Ludwig-Maximilians-Universität München, Butenandtstrasse 5-13, 81377 München, Germany*
[5]*CNR–IOM, Strada Statale 14, km 163.5, Trieste 34149, Italy*
[6]*Laboratoire de Physique des Matriaux et des Surfaces, Université de Cergy-Pontoise, 5 mail Gay-Lussac, 95031 Cergy-Pontoise, France*
[7]*DSM, IRAMIS, Service de Physique de l'Etat Condensé, CEA-Saclay, 91191 Gif-sur-Yvette, France*
[8]*Diamond Light Source, Chilton, Didcot, Oxfordshire OX110DE, United Kingdom*
[9]*Institute of Condensed Matter Physics (ICMP), École Polytechnique Fédérale de Lausanne (EPFL), CH-1015 Lausanne, Switzerland*
[10]*New Technologies-Research Center, University of West Bohemia, Univerzitni 8, 306 14 Pilsen, Czech Republic*
[11]*Università degli Studi di Trieste, Via A. Valerio 2, Trieste 34127, Italy*
[12]*International Faculty, University of Köln, 50937 Köln, Germany*

(Received 15 September 2014; published 4 March 2015)

The prospect of optically inducing and controlling a spin-polarized current in spintronic devices has generated wide interest in the out-of-equilibrium electronic and spin structure of topological insulators. In this Letter we show that only measuring the spin intensity signal over several orders of magnitude by spin-, time-, and angle-resolved photoemission spectroscopy can provide a comprehensive description of the optically excited electronic states in Bi_2Se_3. Our experiments reveal the existence of a surface resonance state in the second bulk band gap that is benchmarked by fully relativistic *ab initio* spin-resolved photoemission calculations. We propose that the newly reported state plays a major role in the ultrafast dynamics of the system, acting as a bottleneck for the interaction between the topologically protected surface state and the bulk conduction band. In fact, the spin-polarization dynamics in momentum space show that these states display macroscopically different temperatures and, more importantly, different cooling rates over several picoseconds.

DOI: 10.1103/PhysRevLett.114.097401 78.47.jd, 73.20.-r, 78.30.-j, 79.60.-i

The possibility of optically inducing a spin-polarized electrical current in topological insulators (TIs) [1–7] has recently raised interest in the out-of-equilibrium properties of these materials [8–17]. The direct measurement of the spin-dependent scattering times and the modification of the spin polarization near the Fermi level (E_F) are of fundamental importance for gaining full control over the optically induced spin current in TIs. However, the study of the spin dynamics of the surface and bulk bands has been hampered by the lack of spin resolution in the time- and angle-resolved photoelectron spectroscopy (TR ARPES) experiments reported in the literature so far [8–17]. Moreover, recent TR ARPES experiments have shown a very complex interplay between the electrons photoexcited in the surface spin-polarized states and in the bulk spin degenerate states [10,18,19]. Understanding in detail the scattering between the bulk and surface states is of fundamental importance for future optospintronic devices, since the bulk states might also be responsible for a net photogalvanic current [5]. Bulk and surface derived states might partially couple within the conduction band projected band gap, thus strongly affecting the electron relaxation times [20]. Our combined experimental and theoretical work aims to unveil the microscopic mechanisms responsible for the interplay between the bulk and surface derived states and the spin-resolved dynamics of Bi_2Se_3 both below and above E_F in the subpicosecond time domain.

In this Letter we report a spin- and time-resolved ARPES (STAR PES) study of the archetypal TI, Bi_2Se_3, optically excited by infrared ultrafast laser pulses. The photoinduced hot carriers exhibit significantly different energy-dependent dynamics for opposite spin channels. Both the equilibrium and out-of-equilibrium spin-resolved band structure and the dynamics of the polarized spin channels are fully benchmarked at 300 and 850 K by relativistic *ab initio* photoemission calculations. The presence of a highly spin-polarized surface resonance state (SRS), with spin polarization opposite to the topologically protected surface state (TSS) and with topologically trivial character, is unveiled.

The complex spin-dynamics texture in reciprocal space is well accounted for by considering two distinct electronic populations in the surface and bulk states that thermalize with two significantly different electronic temperatures and cooling times. The presence of the SRS causes a reduction in the bulk conduction band (BCB) spectral weight at the surface and is proposed as the key mechanism responsible for the very weak interaction between the BCB and the TSS.

Experiments were performed at room temperature, with a combined energy and momentum resolution of ~90 meV and 0.01 $Å^{-1}$. The temporal resolution was ~250 fs. High quality single crystals were cleaved in ultrahigh vacuum (5×10^{-10} mbar). Figure 1(a) shows on a logarithmic scale the measured (left) and calculated (right) spin-resolved energy distribution curves (EDCs). The experimental data were acquired near the TSS Fermi wave vector k_F at $-7°$ along the ΓK high symmetry direction using a 6.2 eV photon energy and s polarization. For more details about the spin-resolved ARPES and the experimental setup, see the Supplemental Material [21]. Red and blue correspond to spin-up and -down, dotted (continuous) line indicates the measured EDCs before (after) the arrival of the 1.55 eV pump pulse at the delays of -1 ps and $+500$ fs, respectively. We associate the spin-polarized peak located at E_F to the TSS. Before optical excitation, both spin EDCs decrease exponentially above E_F, showing a characteristic Fermi Dirac (FD) cutoff. When the system is optically excited, at ~250 meV above E_F the spin polarization is inverted with respect to the TSS, while between 500 and 800 meV, a spin-unpolarized region is observed. In agreement with the helical spin texture of the TSS [1,3,22,23], similar behavior, but with opposite spin, is observed at the opposite k_F. (For more details, see the Supplemental Material [21].)

To reveal the origin of the photoexcited spin texture in momentum space we performed *ab initio* spin-resolved photoemission calculations for 6.2 eV photon energy and s-polarized light, matching the experimental conditions. These calculations are based on the relativistic one-step model. The model, in its spin-density matrix formulation, describes properly the complete spin polarization, i.e., all three components of the spin-polarization vector for each (k_x, k_y) point [21]. The final state is modeled as a so-called time-reversed spin-polarized low-energy electron diffraction (SPLEED) state [24]. The photoemission calculations also account for matrix-element and multiple scattering effects in the initial and final states. Many-body effects are included phenomenologically in the SPLEED calculations, by using a parametrized and weakly energy-dependent complex inner potential, $V_0(E) = V_{0r}(E) + iV_{0i}(E)$ [25]. (For more details, see the Supplemental Material [21], which includes Refs. [26–32].)

The spin EDCs extracted from k-dependent photoemission calculations multiplied by a Fermi-Dirac distribution function are shown in the right-hand side of Fig. 1(a). Dotted (continuous) blue and red lines correspond to an electronic temperature equal to $T_{(-1\,\mathrm{ps})} = 300$ K ($T_{(500\,\mathrm{fs})} = 850$ K), where 850 K is the optimal temperature to reproduce the measured spin integrated intensity (black line) at +500 fs delay. This procedure benchmarks our experimental data, showing whether or not a single electronic distribution is sufficient to reproduce our data.

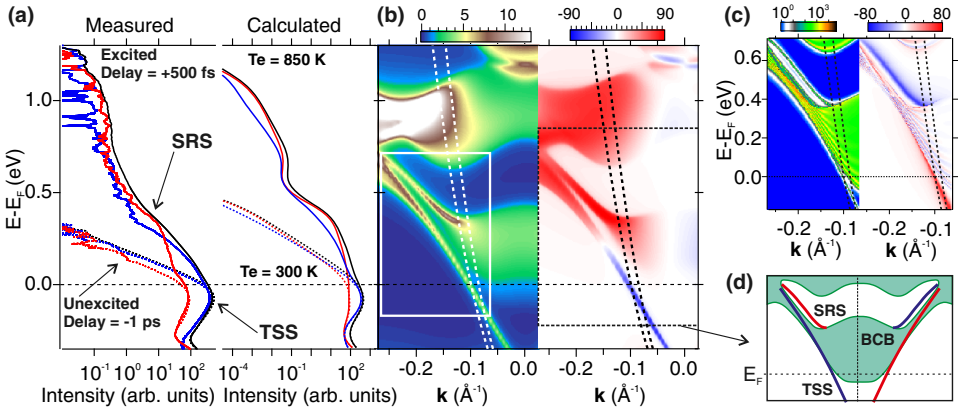

FIG. 1 (color online). (a) Measured (left) and calculated (right) spin-resolved EDCs along the ΓK high symmetry direction close to the TSS k_F of Bi_2Se_3. The TSS and SRS peaks are indicated by arrows. Dotted (continuous) blue and red lines indicate the two opposite spin intensities before (after) optical excitation, while black lines indicate the spin integrated signal. The calculated spin EDC for a sample temperature of $T = 850$ K can account for the change in the relative spin intensity after optical excitation at $E - E_F \sim 250$ meV, attributed to the presence of SRS. (b) Spin integrated (left) and spin-resolved (right) *ab initio* photoemission calculations for Bi_2Se_3 along the ΓK high symmetry direction for 6.2 eV photon energy and s polarization, as in the experiments. Dashed lines indicate the region where the calculated EDCs of (a) were extracted. (c) Spin integrated (left) and spin-resolved (right) calculated ground state electronic properties of Bi_2Se_3 along the ΓK high symmetry. Comparison to the photoemisson calculations within the white rectangle of (b) highlights the photoemission matrix element effects. (d) Schematics of the electronic structure of Bi_2Se_3, showing the TSS and SRS states dispersing across the band gap within the BCB.

Figure 1(b) shows the calculated spin integrated (left) and spin-resolved (right) photoemission intensity along the ΓK high symmetry direction. The dotted lines indicate the region where the EDCs of Fig. 1(a) are integrated. Because of the influence of the light polarization on the photoelectron spin, the ground state calculations are also required to completely interpret the photoemission spin polarization [22,23,33]. Figure 1(c) presents the ground state calculations over a selected region [see Fig. 1(b), white rectangle]. Beside the TSS and the BCB, an additional spin-polarized surface state, dispersing in a bulk projected band gap, is observed in the experimental data and reproduced by the calculations. The surface character of this state, never reported before, differs from the TSS, and we identify it as a surface resonance of bulk states. Because of the appearance of the SRS, the BCB loses spectral weight close to the surface in favor of the resonance. Noticeably, the SRS and TSS have opposite spin polarization, but the former is topologically *trivial*. Figure 1(d) schematizes the electronic properties of Bi_2Se_3, with the spin-polarized TSS and SRS dispersing in two different projected band gaps of the BCB.

The photoemission spin structure reported in Fig. 1(b) shows that for *s*-polarized light the TSS and SRS photoelectron spin is opposite to the ground state polarization shown in Fig. 1(c). This is a consequence of the strong spin-orbit coupling combined with the orbital-dependent photoexcitation probabilities [33]. Furthermore, even though the BCB ground state is spin unpolarized, the BCB reveals a photoelectron spin polarization, increasing from zero at E_F to appreciable polarization at $E - E_F \sim 0.9$ eV. This is a consequence of the partial hybridization between the SRS and the TSS states which characterizes the equilibrium electronic properties of Bi_2Se_3 in the ground state.

The measured spin inversion at $E - E_F \sim 250$ meV, as observed in Fig. 1(a), is assigned to the SRS, having a spin polarization opposite to the TSS. The polarization detected at high energy ($E - E_F > 1$ eV) arises from the top side of the BCB, whose weak spin polarization is visible in Fig. 1(b). Finally, the spin-unpolarized weak signal between 500 and 800 meV corresponds to the energy region of the projected band gap.

At first glance, the comparison between the experimental and calculated spin EDCs in Fig. 1(a) might suggest the possibility of describing the optically excited EDCs by a single thermalized electronic distribution populating the excited spin states. Next, we show that this picture is not fully satisfactory. To address this issue the characteristic relaxation times for both spin states above E_F are compared.

Figure 2(a) shows the spin-resolved intensity difference EDCs (ΔI) measured at 500 fs delay after excitation. The temporal evolution of ΔI is presented in Fig. 2(b) for three energy regions [black arrows in Fig. 2(a)]. By fitting a single exponential decay function to the data, we extract the spin-dependent relaxation times. Slightly above E_F

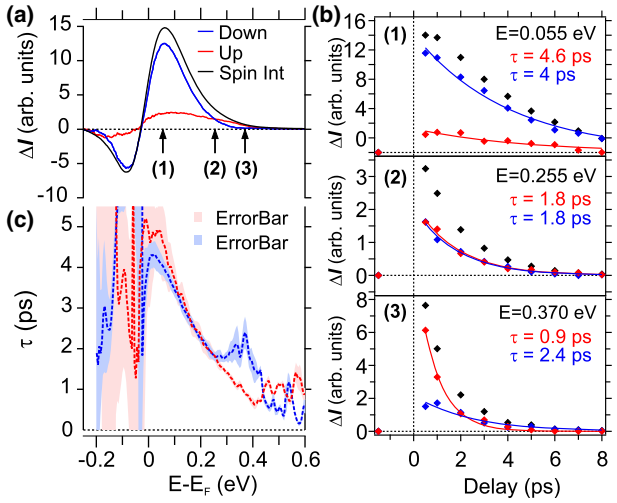

FIG. 2 (color online). (a) Delta spin (red and blue) and spin integrated (black) EDCs obtained as the difference between the signal measured after and before optical excitation. (b) Time evolution of the spin-up (red), spin-down (blue), and spin integrated (black) intensity integrated as a function of the delay time within the energy region indicated by three arrows in (a), respectively, at $E - E_F = 0.055$, 0.255, 0.370 eV. From the exponential fit of the intensity decays, we infer the spin-dependent relaxation times τ displayed in each panel. (c) Spin-dependent relaxation times for the spin-up (red) and spin-down (blue) as a function of the binding energy for the entire measured band dispersion.

(0.055 eV), the intensity of the two opposite spins have comparable characteristic relaxation times, $\tau_{red} = 4.6$ ps and $\tau_{blue} = 4.0$ ps. The same behavior is observed for photoelectron kinetic energies up to 0.255 eV (second region), where the two spin populations have the same intensity and $\tau_{red} = \tau_{blue} = 1.8$ ps. On the contrary, at 0.370 eV (third region) a faster relaxation for the majority spin component (spin-up, in red) is clearly observed, $\tau_{red} = 0.9$ ps and $\tau_{blue} = 2.4$ ps.

Figure 2(c) displays the spin-dependent decay time over the full energy range. These findings, along with the spin-polarized photoemission intensities near E_F, set the boundary conditions for optically controlling the spin-polarized currents in TIs. In the proximity of E_F the decay times are comparable [21]. By taking advantage of the large signal-to-noise ratio of our time-of-flight detector [34], we observe that in the energy region 300–500 meV above E_F the minority spin components persist for longer times. This behavior suggests that the out-of-equilibrium electronic properties cannot be described in terms of a single thermalized electronic population. In fact, for this case we would expect the same τ for both spin components along with a monotonic decrease of τ as a function of the binding energy (see Supplemental Material [21] and ref. [11]). Hence, a single thermalized electronic population cannot account for the fine structure of τ that is observed for $E - E_F > 0.35$ eV: the different spin relaxation times and

the local maximum in the blue spin channel. To reproduce these features a superposition of two distinct thermalized electronic populations must be taken into account.

The photoemission signal at 500 fs, shown in Fig. 3(a), already suggests the existence of two distinct electronic populations. Up to 0.4 eV, the surface contribution associated with the TSS and SRS dominates, with an effective electronic temperature $T_S(500\ \mathrm{fs}) \sim 850$ K. However, at higher binding energies the photoemission intensity does not drop according to a 850 K Fermi-Dirac distribution. This is clearly evidenced by the mismatch between the experimental data and the calculated spin EDCs represented by the black dashed lines in Fig. 3(a). The measured spin EDCs display a tail at $E - E_F > 0.6$ eV characterized by a small spin-unpolarized DOS (2 orders of magnitude smaller than the surface DOS). This second electronic population has an effective temperature of $T_B(500\ \mathrm{fs}) = 2300$ K. The energy position of this electronic tail suggests that the second electronic subsystem is a *hot* electron gas excited in the high-energy side of the BCB.

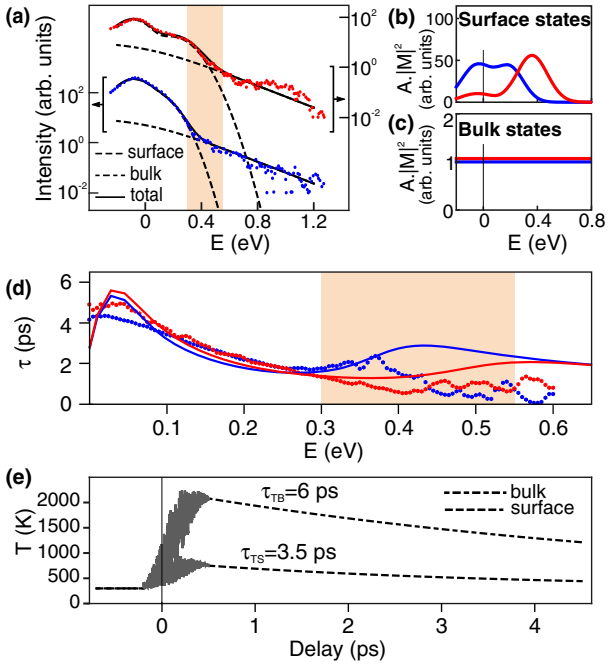

FIG. 3 (color online). (a) Experimental (points) and theoretical (full line) spin-resolved photoemission intensities, shifted for ease of visualization, for the red and blue spin channels. The contributions from the surface and bulk states to the total theoretical photocurrent are indicated by dashed and dash-dotted lines, respectively. The orange area highlights the bulk versus surface crossover energy range. (b),(c) Optimized spectral function A multiplied by the photoemission matrix element $|M|^2$ of the surface states (b) and the bulk states (c) (see Supplemental Material for details about the optimization and fit [21]). (d) Experimental (points) and theoretical (full line) energy- and spin-resolved relaxation times of the photocurrent intensity. (e) Temporal evolution of the electronic temperatures for the surface (dashed line) and bulk states (dash-dotted line). The gray area indicates the time range before electronic thermalization.

The spin- and time-resolved photoemission data further support the presence of two noninteracting electronic systems. Hence, we model the photoemission spectrum as the sum of two independent contributions associated with the surface (S) and bulk (B):

$$I_{\mathrm{tot}}^{\mathrm{PES}}(\sigma, E, t) = A_S(\sigma, E)|M_S(\sigma, E)|^2 f_{\mathrm{FD}}(E, T_S(t), \mu_S(t)) + A_B(\sigma, E)|M_B(\sigma, E)|^2 f_{\mathrm{FD}}(E, T_B(t), 0), \quad (1)$$

where $A_{S,B}$ are the amplitudes of the surface and bulk states, $M_{S,B}$ are the matrix element, and $T_S(t) = T_S(\infty) + \Delta T_S \exp[-t/\tau_{TS}]$ and $\mu_S(t) = \mu_S(\infty) + \Delta\mu_S \exp[-t/\tau_{\mu S}]$ are the time evolution of the electronic temperature and the chemical potential of the surface states, respectively. For the bulk states, $T_B(t) = T_B(\infty) + \Delta T_B \exp[-t/\tau_{TB}]$. To a good approximation, the chemical potential of the bulk can be kept fixed. The relaxation times τ_{TS} and τ_{TB} for the temperature of the surface and bulk states, respectively, are left as free parameters.

A fitting procedure is used to extract the energy and spin-resolved relaxation times. Figures 3(b) and 3(c) show the $A_i(\sigma, E)|M_i(\sigma, E)|^2$, with $i = S, B$ functions. The two are optimized starting from the *ab initio* relativistic calculations, in order to better reproduce the experimental spin EDCs after optical excitation (see Supplemental Material [21]).

Figures 3(a) and 3(d) show that, in the energy region close to E_F, the time-resolved spin ARPES signals are dominated by the surface state contribution with the bulk DOS 2 orders of magnitude smaller, while for $E - E_F > 600$ meV the signal is dominated by the bulk states, with a larger electronic temperature (see Supplemental Material [21]). Interestingly, for $E \sim E_F$ and $E - E_F > 600$ meV, the two spin channels show the same relaxation dynamics, regardless of the different spin polarization of the surface and bulk states.

In contrast, in the region $300 > E - E_F > 550$ meV, highlighted by the orange area in Fig. 3(d), both subsystems contribute to the total photoemission intensity. The surface state contribution to the blue (red) spin component is smaller (larger) than the bulk one. This results in different spin dynamics. In particular, the local maximum in the characteristic relaxation time of the blue spin component results from the larger relaxation times of the bulk states. Figure 3(d) shows the decay times obtained by the numerical fitting of Eq. (1), where $\mu_S(0) = 0.02$ eV, $\tau_{\mathrm{TS}} = 3.5$ ps, $\tau_{\mu S} = 1.7$ ps, and $\tau_{\mathrm{TB}} = 6$ ps were used. Remarkably, the values obtained for the TSS are comparable to those reported in previous TR ARPES studies [8,10,11], whereas the relaxation time of the bulk states is about twice that of the surface states.

Figure 3(e) clearly shows that the surface (dashed line) and bulk states (dash-dotted line) behave as independent electronic populations that thermalize, after optical excitation, to two different temperatures. Subsequently, they relax back to equilibrium with different τ, τ_{TS}, and τ_{TB}. Hence, the TSS and the BCB do not show any significant electron-electron scattering in this time scale. We ascribe this unexpectedly weak coupling to the presence of the SRS reducing the presence of the BCB in the region close to the surface. This then acts as a bottleneck by scattering directly with the TSS, but not allowing any hot electron diffusion towards the inner bulk. The reduced coupling between bulk and surface states manifests in largely different relaxation times even at room temperature. These findings enhance previous spin integrated studies reporting a small difference between T_S and T_B only below the material Debye temperature [10].

In summary, we have investigated the out-of-equilibrium spin and electronic properties of Bi_2Se_3. The spin resolution combined with the very high signal-to-noise ratio of the time-of-flight spectrometer enables us to reveal novel aspects of the spin and electron dynamics in TIs. We fully map the band structure in the unoccupied density of states and we identify a spin-polarized SRS with topologically trivial character. The surface resonance is shown to play a key role in the spin-dependent relaxation of the photoexcited electrons, by partially decoupling the BCB from the TSS. In fact, by accessing the spin relaxation dynamics we have shown that electrons in the surface and bulk states are weakly coupled even at room temperature, and within the first ~8 ps after the optical excitation they can be described as two independent electronic populations with different temperature and relaxation dynamics. These results unveil the complexities of the spin scattering processes in TIs.

In the future, our findings may have important implications for the optical control of spin currents in TIs. The newly discovered SRS, which we suggest is responsible for the weak coupling between the BCB and the TSS at room temperature, points towards the possibility of independently manipulating the surface and the bulk spin states.

C. C and A. C. contributed equally to this work. This work was funded by the FERMI project of Elettra-Sincrotrone Trieste, partially supported by the Ministry of University and Research (Grants No. FIRB-RBAP045JF2 and No. FIRBRBAP06AWK3). J. B., H. E., and J. M., members of the COST action MP1306 EUSpec, were supported by the Deutsche Forschungsgemeinschaft (DFG) within SPP1666, by the BMBF (Project 05K13WMA) and CENTEM (CZ.1.05/2.1.00/03.0088). We thank Phil Rice for technical support and Diamond Light Source for providing the laser facilities to perform the experiments.

*fulvio.parmigiani@elettra.eu

[1] M. Z. Hasan and C. L. Kane, Rev. Mod. Phys. **82**, 3045 (2010).
[2] X.-L. Qi and S.-C. Zhang, Rev. Mod. Phys. **83**, 1057 (2011).
[3] D. Hsieh, Y. Xia, D. Qian, L. Wray, J. H. Dil, F. Meier, J. Osterwalder, L. Patthey, J. G. Checkelsky, N. P. Ong *et al.*, Nature (London) **460**, 1101 (2009).
[4] D. Hsieh, Y. Xia, L. Wray, D. Qian, A. Pal, J. H. Dil, J. Osterwalder, F. Meier, G. Bihlmayer, C. L. Kane *et al.*, Science **323**, 919 (2009).
[5] J. W. McIver, D. Hsieh, H. Steinberg, P. Jarillo-Herrero, and N. Gedik, Nat. Nanotechnol. **7**, 96 (2012).
[6] Y. Xia, D. Qian, D. Hsieh, L. Wray, A. Pal, H. Lin, A. Bansil, D. Grauer, Y. S. Hor, R. J. Cava *et al.*, Nat. Phys. **5**, 398 (2009).
[7] Z. Xie, S. He, C. Chen, Y. Feng, H. Yi, A. Liang, L. Zhao, D. Mou, J. He, Y. Peng *et al.*, Nat. Commun. **5**, 3382 (2014).
[8] J. A. Sobota, S. Yang, J. G. Analytis, Y. L. Chen, I. R. Fisher, P. S. Kirchmann, and Z.-X. Shen, Phys. Rev. Lett. **108**, 117403 (2012).
[9] M. Hajlaoui, E. Papalazarou, J. Mauchain, G. Lantz, N. Moisan, D. Boschetto, Z. Jiang, I. Miotkowski, Y. P. Chen, A. Taleb-Ibrahimi *et al.*, Nano Lett. **12**, 3532 (2012).
[10] Y. H. Wang, D. Hsieh, E. J. Sie, H. Steinberg, D. R. Gardner, Y. S. Lee, P. Jarillo-Herrero, and N. Gedik, Phys. Rev. Lett. **109**, 127401 (2012).
[11] A. Crepaldi, B. Ressel, F. Cilento, M. Zacchigna, C. Grazioli, H. Berger, P. Bugnon, K. Kern, M. Grioni, and F. Parmigiani, Phys. Rev. B **86**, 205133 (2012).
[12] M. Hajlaoui, E. Papalazarou, J. Mauchain, Z. Jiang, I. Miotkowski, Y. Chen, A. Taleb-Ibrahimi, L. Perfetti, and M. Marsi, Eur. Phys. J. Spec. Top. **222**, 1271 (2013).
[13] A. Crepaldi, F. Cilento, B. Ressel, C. Cacho, J. C. Johannsen, M. Zacchigna, H. Berger, P. Bugnon, C. Grazioli, I. C. E. Turcu *et al.*, Phys. Rev. B **88**, 121404 (2013).
[14] Y. H. Wang, H. Steinberg, P. Jarillo-Herrero, and N. Gedik, Science **342**, 453 (2013).
[15] M. Hajlaoui, E. Papalazarou, J. Mauchain, L. Perfetti, A. Taleb-Ibrahimi, F. Navarin, M. Monteverde, P. Auban-Senzier, C. Pasquier, N. Moisan *et al.*, Nat. Commun. **5**, 3003 (2014).
[16] J. A. Sobota, S.-L. Yang, D. Leuenberger, A. F. Kemper, J. G. Analytis, I. R. Fisher, P. S. Kirchmann, T. P. Devereaux, and Z.-X. Shen, J. Electron Spectrosc. Relat. Phenom. **195**, 249 (2014).
[17] D. Niesner, S. Otto, V. Hermann, T. Fauster, T. V. Menshchikova, S. V. Eremeev, Z. S. Aliev, I. R. Amiraslanov, M. B. Babanly, P. M. Echenique *et al.*, Phys. Rev. B **89**, 081404 (2014).
[18] J. A. Sobota, S.-L. Yang, D. Leuenberger, A. F. Kemper, J. G. Analytis, I. R. Fisher, P. S. Kirchmann, T. P. Devereaux, and Z.-X. Shen, Phys. Rev. Lett. **113**, 157401 (2014).
[19] S. Sim, M. Brahlek, N. Koirala, S. Cha, S. Oh, and H. Choi, Phys. Rev. B **89**, 165137 (2014).
[20] J. A. Sobota, S.-L. Yang, A. F. Kemper, J. J. Lee, F. T. Schmitt, W. Li, R. G. Moore, J. G. Analytis, I. R. Fisher, P. S. Kirchmann *et al.*, Phys. Rev. Lett. **111**, 136802 (2013).

[21] See Supplemental Material at http://link.aps.org/supplemental/10.1103/PhysRevLett.114.097401 for a detailed description of the experimental setup and the equilibrium spin ARPES results, along with a description of the ab initio calculations and the model describing the out-of-equilibrium spin intensity.
[22] C. Jozwiak, C.-H. Park, K. Gotlieb, C. Hwang, D.-H. Lee, S. G. Louie, J. D. Denlinger, C. R. Rotundu, R. J. Birgeneau, Z. Hussain *et al.*, Nat. Phys. **9**, 293 (2013).
[23] Z.-H. Zhu, C. Veenstra, S. Zhdanovich, M. P. Schneider, T. Okuda, K. Miyamoto, S.-Y. Zhu, H. Namatame, M. Taniguchi, M. W. Haverkort *et al.*, Phys. Rev. Lett. **112**, 076802 (2014).
[24] J. Braun, Rep. Prog. Phys. **59**, 1267 (1996).
[25] J. B. Pendry, *Low Energy Electron Diffraction* (Academic, New York, 1974).
[26] C. Caroli, D. Lederer-Rozenblatt, B. Roulet, and D. Saint-James, Phys. Rev. B **8**, 4552 (1973).
[27] G. Borstel, Appl. Phys. A **38**, 193 (1985).
[28] S. V. Halilov, E. Tamura, D. Meinert, H. Gollisch, and R. Feder, J. Phys. Condens. Matter **5**, 3859 (1993).
[29] G. Hilgers, M. Potthoff, N. Müller, U. Heinzmann, L. Haunert, J. Braun, and G. Borstel, Phys. Rev. B **52**, 14859 (1995).
[30] T. Fujikawa and H. Arai, J. Electron Spectrosc. Relat. Phenom. **123**, 19 (2002).
[31] J. B. Pendry, Surf. Sci. **57**,679 (1976).
[32] J. Braun, K. Miyamoto, A. Kimura, T. Okuda, M. Donath, H. Ebert, and J. Minár, New J. Phys. **16**,015005 (2014).
[33] J. Sánchez-Barriga, A. Varykhalov, J. Braun, S.-Y. Xu, N. Alidoust, O. Kornilov, J. Minár, K. Hummer, G. Springholz, G. Bauer *et al.*, Phys. Rev. X **4**, 011046 (2014).
[34] C. M. Cacho, S. Vlaic, M. Malvestuto, B. Ressel, E. A. Seddon, and F. Parmigiani, Rev. Sci. Instrum. **80**, 043904 (2009).